Printable Nanophotonic Devices *via* Holographic Laser Ablation

Qiancheng Zhao,[†,§] Ali K. Yetisen,[‡,§] Aydin Sabouri,[†] Seok Hyun Yun,[‡] and Haider Butt[*,†]

[†]Microengineering and Nanotechnology Laboratory, School of Mechanical Engineering, University of Birmingham, Edgbaston, Birmingham B15 2TT, United Kingdom and [‡]Harvard Medical School and Wellman Center for Photomedicine, Massachusetts General Hospital, 50 Blossom Street, Boston, Massachusetts 02114, United States. [§]Q.Z. and A.K.Y.: These authors contributed equally.

ABSTRACT Holography plays a significant role in applications such as data storage, light trapping, security, and biosensors. However, conventional fabrication methods remain time-consuming, costly, and complex, limiting the fabrication of holograms and their extensive use. Here, we demonstrate a single-pulse laser ablation technique to write parallel surface gratings and Fresnel zone plates.

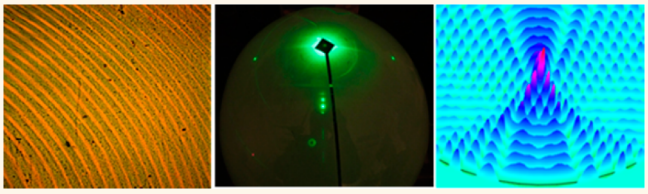

We utilized a 6 ns high-energy green laser pulse to form interference patterns to record a surface grating with 820 nm periodicity and asymmetric zone plate holograms on 4.5 nm gold-coated substrates. The holographic recording process was completed within seconds. The optical characteristics of the interference patterns have been computationally modeled, and well-ordered polychromatic diffraction was observed from the fabricated holograms. The zone plate showed a significant diffraction angle of 32° from the normal incident for the focal point. The nanosecond laser interference ablation for rapid hologram fabrication holds great potential in a vast range of optical devices.

KEYWORDS: holography · laser interference · zone plates · diffraction gratings · lenses

Holograms have applications in spectroscopy, telecommunication, light trapping, security systems, and biosensors.[1−9] A hologram is an optical image typically stored in a two- or three-dimensional (2D or 3D) medium of interference patterns formed by coherent laser beams. The image consists of a structure with varying density or profile that reconstructs a wavefront by means of diffraction.[10] Historically, 3D holograms have been recorded using silver halide chemistry and photopolymers.[11] In silver halide holograms, the image is recorded in a laser light sensitive emulsion, followed by photographic development.[7] While photopolymers are recorded in the same mode, they can be cured by heat treatment or ultraviolet/visible light exposure.[12] Practical approaches can be realized by recording images in photoresist, which can be transformed into a nickel surface relief grating for embossing holograms in hydrophobic polymers.[13] The use of photoresist requires high-cost and customized equipment for fabricating the master holograms. Surface gratings can also be written by complex techniques such as E-beam lithography (EBL) and focused ion beam (FIB) milling.[14−16] However, these approaches are high-cost, low-throughput, and labor intensive.[17] To overcome these limitations, direct laser interference patterning (DLIP) in split-beam off-axis mode has been developed to fabricate surface patterns.[18] This approach involves laser pulses (~300 mJ/cm^2) to selectively modify thin films made out of polymers, aluminum zinc oxide, nickel, and steel.[19,20] For example, the use of a frequency-quadrupled diode-pumped solid-state laser (6 ns, 266 nm, 20 mJ) allowed direct interference patterning of light-emitting fluorene polymer.[21] In these approaches, the laser pulse was split into multiple beams, which were focused by identical lenses on the sample surface. This approach known as off-axis interference patterning requires accurate symmetric and interferometric alignment of multiple laser beams. The development of customizable single-beam patterning techniques without requiring a complex optical setup remains a challenge in producing optical elements.

Here, we demonstrate a one-step rapid holographic recording technique, in which a nanosecond laser pulse is used to engineer diffraction patterns on transparent substrates coated by light-absorbing materials. In laser light patterning, a grating can be produced by the intensity distribution of

* E-mail: h.butt@bham.ac.uk.

Received for review May 26, 2015 and accepted August 22, 2015.

Published online
10.1021/acsnano.5b03165

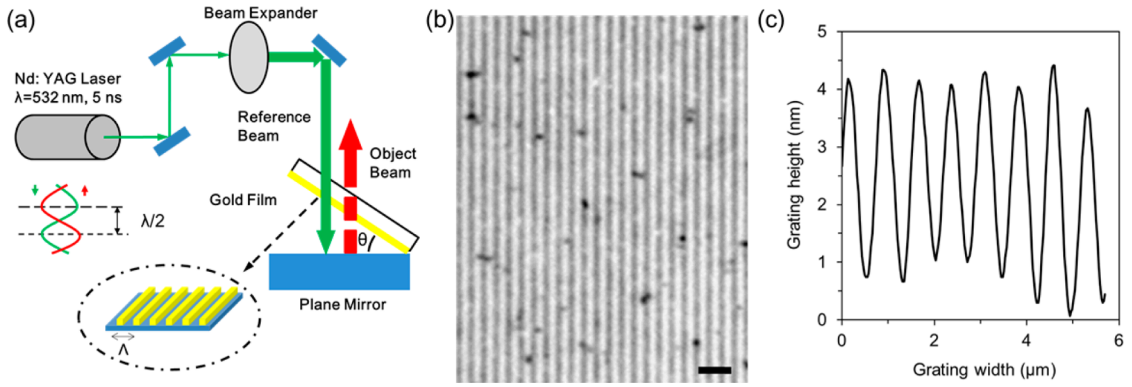

Figure 1. Fabrication of the holograms through nanosecond laser light interference. (a) Schematic of the surface hologram recording setup. A Nd:YAG pulsed laser beam (λ = 532 nm, 350 mJ) travels through the beam expander and is reflected back from an object. (b) Microscope image of gold surface grating showing parallel lines. Scale bar = 2 μm. (c) Diffraction grating periodicity of ~820 nm.

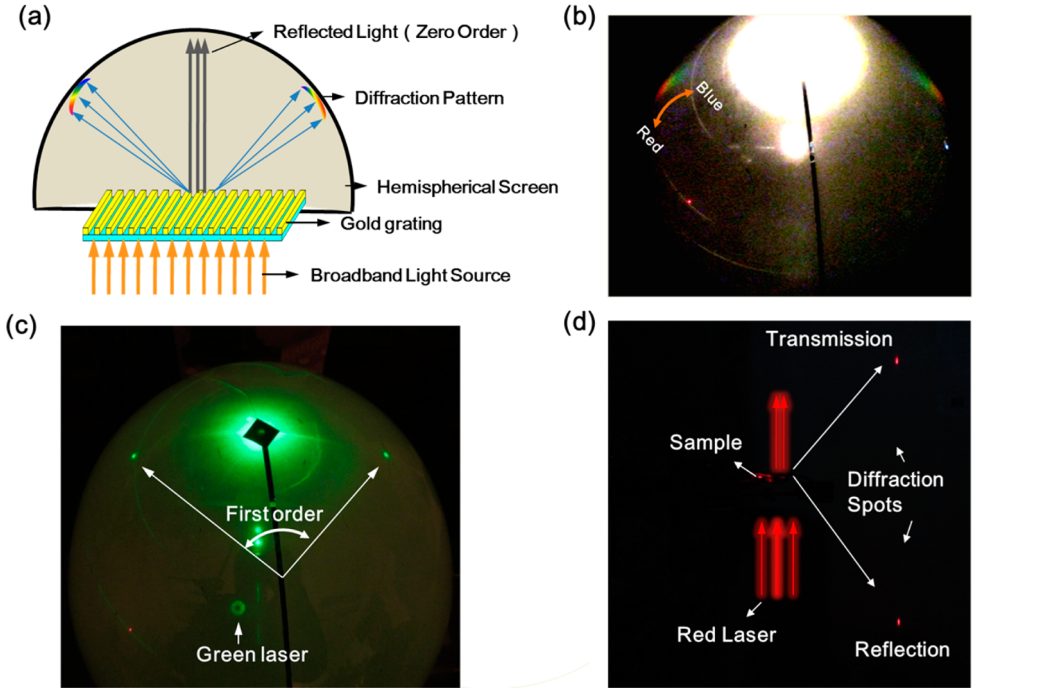

Figure 2. Optical characterization of the diffraction grating fabricated *via* laser ablation. (a) Schematic of an integrating sphere employed to capture the diffraction pattern. (b) Diffraction pattern obtained by illumination of a broadband white light on a semitransparent hemispherical screen (r = 15 cm). (c) Diffraction spots in transmission mode by shining laser light (532 nm) perpendicular to surface grating. (d) Diffraction spots displayed on a plane screen in both transmission and reflection modes.

interference directed to a coated surface. Unlike silver halide holography, the collimated laser ablation is a physical procedure in which the high peak power of the laser is capable of selectively removing a region of the coated layer determined by the ablation threshold of the light-absorbing material. The optical properties of the formed pattern depend on the pulse duration, localized energy of the laser beam, and any absorption of the ablated material. With the highly localized energy of the laser beam directly ablating the material, an optical device can be fabricated within seconds. In the present work, we present parallel surface gratings and asymmetrical Fresnel zone plates (FZPs) to demonstrate the simplicity and high efficiency of nanosecond pulsed laser ablation holography.

RESULTS

The peak energy of the Nd:YAG laser beam (λ = 532 nm, 6 ns) was set to 10 mJ with a spot area of 1 cm^2 after the beam expander. The laser beam directly patterned the gold-coated sample positioned with a tilt angle from the surface plane of an object (*i.e.*, plane mirror), which was perpendicular to the incident direction (Figure 1a). The interference occurred between the two laser beams traveling in opposite directions, resulting in a well-ordered grating. The period of the

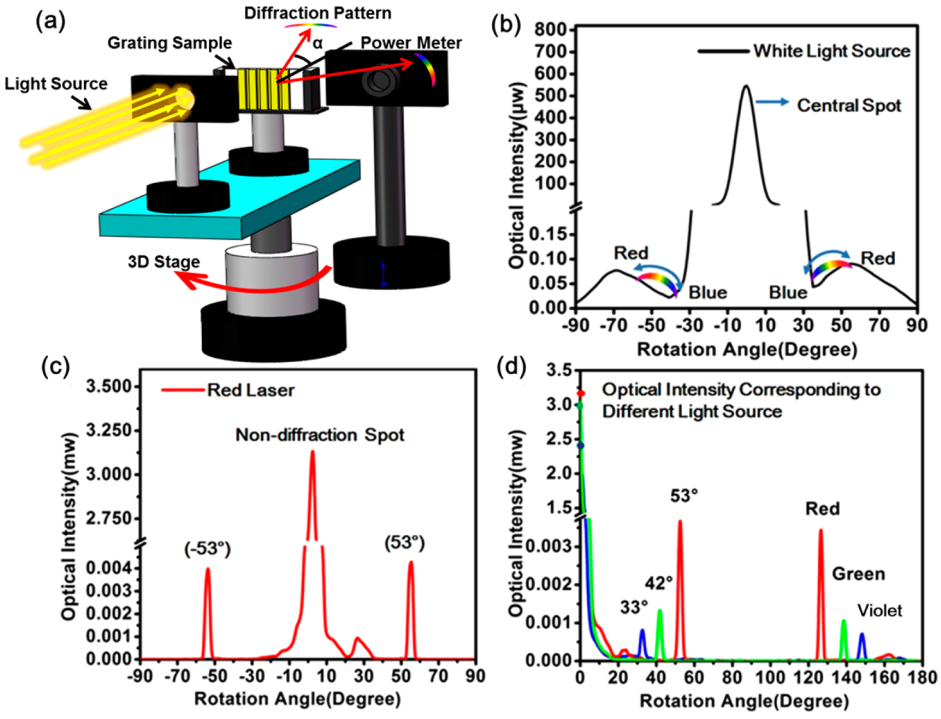

Figure 3. Angle-resolved measurements of the diffraction grating fabricated *via* laser ablation. (a) Schematic of 3D rotational stage setup for the measurements of the optical intensity. (b) Optical intensity distribution by normal incident white light as a function of 180° rotation. (c) Diffracted optical intensity distribution by a laser beam (650 nm) illumination in transmission mode according to rotational angle. (d) Diffracted optical intensity distribution in response to 455, 532, and 650 nm light in both transmission and reflection mode corresponding to rotational angle.

grating was determined by the incident wavelength (λ) and tilt angle (θ) of the sample with respect to normal incidence. The constructive interference occurred at intervals of $\lambda/2$, showing the effect of a stationary wave. Thus, the period for the ablated gratings is

$$\Lambda = \frac{\lambda}{2 \sin\theta} \quad (1)$$

Figure 1b shows a microscope image of the surface grating sample ablated at $\theta = 20°$; the periodicity was measured as 820 nm (Figure 1c), which is in accordance with the theoretically calculated grating periodicity of 778 nm. The difference may be attributed to the simplicity of the laser setup. Linear gratings periods of 3052, 1532, and 1028 nm can be obtained by patterning the gold layer at tilt angles of 5°, 10°, and 15° from the mirror surface plane, respectively.

Figure 2a illustrates the interrogation setup for the optical characterization of the grating. The diffraction pattern for the ablated grating sample is shown in Figure 2b–d by shining different light beams vertically. A well-ordered rainbow was observed by using incident broadband white light with red diffracted at a higher angle and blue at a lower angle (Figure 2b). For monochromatic laser incidence, the diffraction patterns were concentrated spots instead of broadband ribbons (Figure 2c). Diffracted spots in both transmission and reflection modes were visualized in forward and backward directions by normal incident red laser light (Figure 2d).

The diffraction angles and efficiencies for different monochromatic laser sources were studied by optical intensity measurements. The grating sample was placed perpendicularly to the light beam on a 3D rotational stage (Figure 3a). An optical power meter was located in alignment with the collimated light source to allow the measurement of optical intensity. Figure 3b–d shows the diffracted optical intensity distribution as a function of 180° rotation. Two broadband peaks (from 35° to ~60°) were observed symmetrically from both sides of a central zero-order spot, where the diffraction pattern was in agreement with Figure 2b. The diffraction spots were visualized in the range of −90° to +90° with blue diffracted at lower angles and red at higher angles. The diffraction angles for blue, green, and red were measured to be 33°, 42°, and 53°, respectively, which correspond to the grating equation (eq 1). The diffraction efficiency for the incident red laser was experimentally measured to be 0.54% by adding the two transmission spots and two reflection spots (Figure 3c). Both transmission and reflection diffractive spots contribute equally to the total diffraction efficiency. The diffracted optical intensity distribution for each wavelength is shown in Figure 3d.

We demonstrate the utilization of nanosecond laser ablation of surface holograms by producing an asymmetric FZP on a 4.5 nm gold-coated transparent substrate. The reflective object was replaced by a

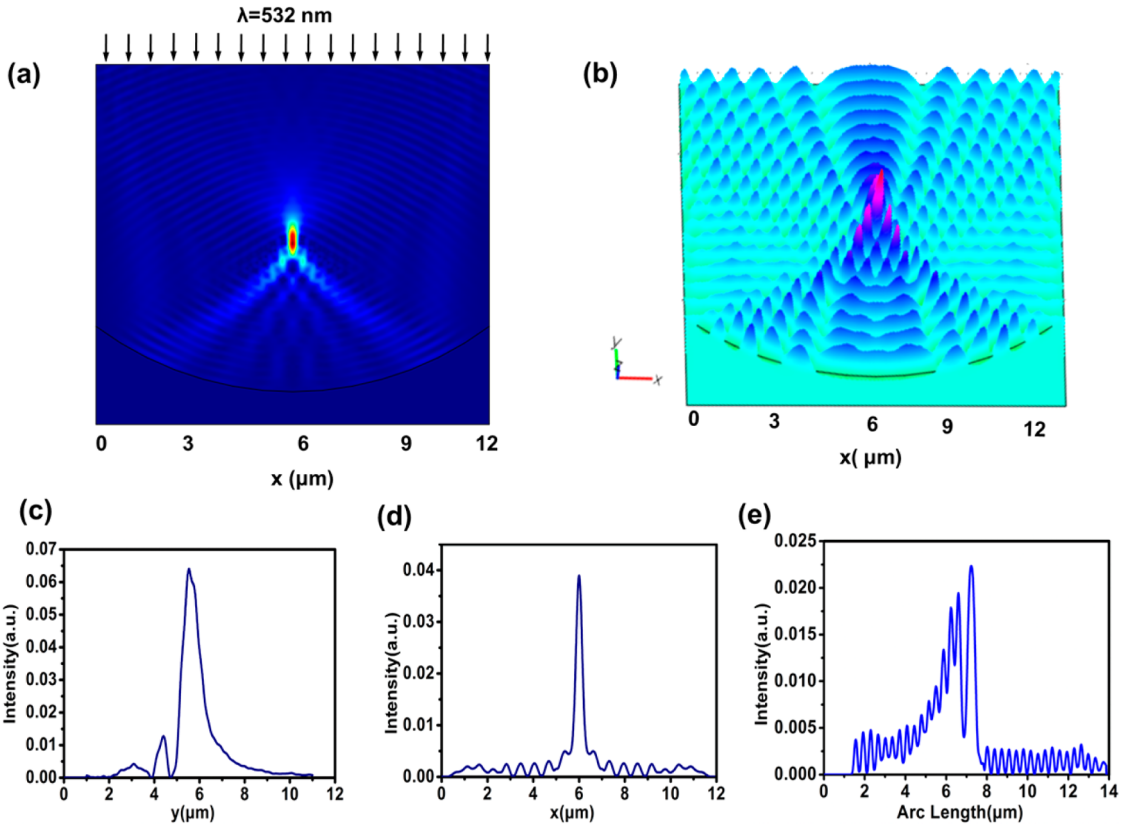

Figure 4. Simulated optical spectra of light interference using a concave mirror. (a) 2D image of interference intensity distribution reflected by a concave mirror. (b) 3D view of the electric field propagation showing the focusing effect. Intensity distribution plots along the (c) *y*-axis and (d) *x*-axis at the focal plane. (e) Intensity distribution at a titled plane of 30°.

concave mirror, which had a diameter and radius of curvature of 25 and 62 mm, respectively. A strong interference occurred between the collimated incident beam and multiple beams reflected from the concave mirror. During recording of the reflection hologram, the sample was set at a tilt angle of 30° from the surface plane. Figure S1 shows the schematic setup for preparing the FZP hologram. To analyze the intensity distribution produced by the interference of multiple laser beams throughout the concave mirror, a computational simulation was performed using the finite element method. Because of the large computational memory and simulation time required by the actual model, a 2000× smaller simulation model was modeled. In the simulation, a 2D model was set up and the electromagnetic field intensity distribution was calculated by inducing a plane wave (λ = 532 nm) incident upon the concave mirror. The intensity distribution produced by the concave mirror was simulated to visualize the interference effect. Figure 4a,b shows the intensity distribution, where a circular interference pattern is observed.

The simulation results show a focal plane produced by the focusing effect of a concave mirror. According to Snell's law, the focal length of a typical concave mirror can be defined as half of the radius of curvature regardless of any focusing errors. Figure 4c shows that the focal plane was at $y = \sim 5.5\ \mu$m, which was identical to the theoretical focal length for a concave mirror with 11 μm curvature radius. Figure 4d shows the intensity distribution along the *x*-axis at the focal plane, and a high-intensity focal point was observed. The profile was symmetrical about the focal point. The 2D interference intensity at 30° tilt angle was also analyzed as a result of the incident and reflected beams. In contrast to the focusing effect at the focal plane, the intensity distribution at a tilted plane of 30° showed an asymmetric power flow distribution from the center (Figure 4e). The intensity of interference peaks decreased from one side to the other. This asymmetric interference patterns when used for ablation of a thin gold film produces an asymmetrical FZP.

The dimensions and surface morphology of the thin gold layer on the glass substrate were analyzed using optical microscopy and atomic force microscopy (AFM). A plate with radial zones alternating from gold circles (opaque zones) to transparent zones (substrate) was observed, and the radius of the outmost zone was measured to be ~2 cm in Figure 5a. Figure 5b shows a magnified region of the FZP, suggesting that the width of the zones decreased farther from the center, which was in agreement with simulation results. The zones were spaced so that the diffracted light constructively interferes at a focus region. Figure S2 shows additional

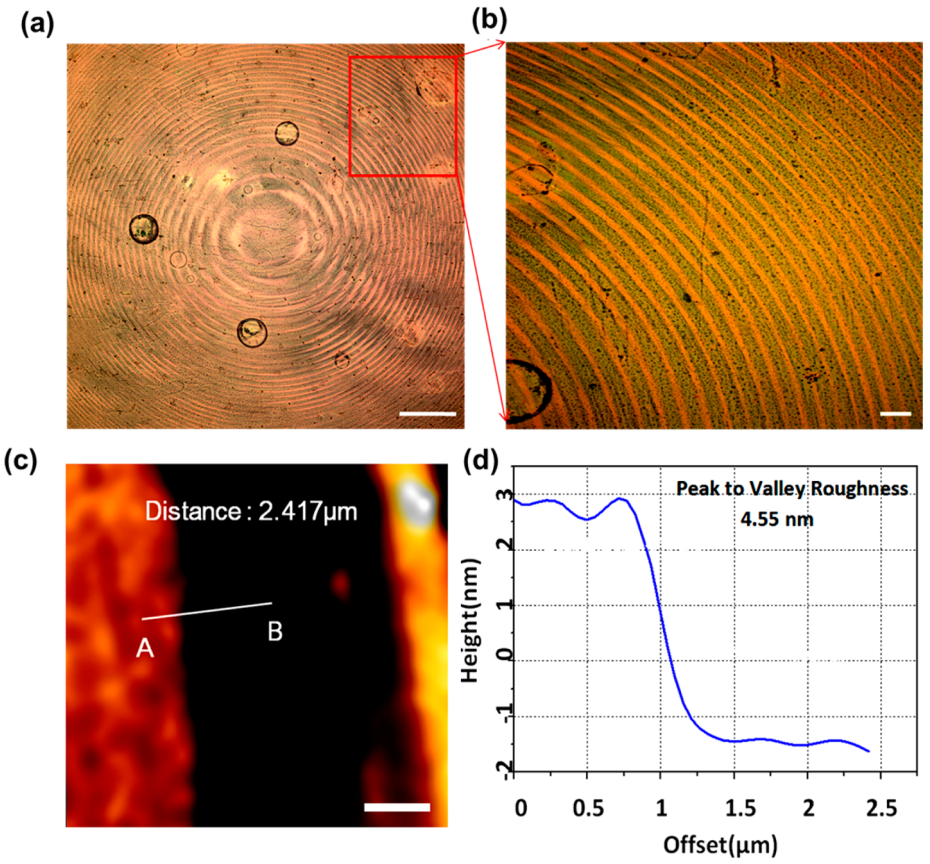

Figure 5. Optical microscopy and AFM characterization of the holographic FZP fabricated *via* laser ablation. (a) An image of the FZP. Scale bar = 200 μm. (b) Magnified microscope image for FZP region in panel a. Scale bar = 20 μm. (c) AFM surface profile for a gold-substrate outer zone. Scale bar = 1 μm. (d) Cross section height profile for segment AB in panel c.

optical microscopy images of the FZP. The dimensions of the zones varied from about a 100 μm (in the center) to few hundred nanometers (at the edge of the lens). Fabricating such as a lens using techniques like E-beam or FIB will clearly be very expensive, time-consuming, and labor intensive. Figure 5c shows an AFM image of a typical outer zone; points A and B on the segment correspond to the gold and substrate regions, respectively. The cross section topography for segment AB is shown by a plot of height profile (Figure 5d). The average height was 4.55 nm, and a side wall tilt was observed at the gold−substrate boundary.

To study the focusing effect and observe diffraction spectra of the holographic FZP, broadband white light was shone upon the lens (Figure S3a). The diffraction pattern for the asymmetrical FZP hologram is shown in Figure S3b. Distinct from conventional symmetric FZPs which focus an incident ray straight along the optical axis, the diffraction pattern for the asymmetric FZP showed a significant diffracted angle, α, to the normal propagation direction. This differentiated the diffracted rainbow from the strong nondiffracted background (zero order). The diffraction image also exhibited a well-ordered spectral rainbow in high contrast ranging from blue to red in both transmission and reflection.

The diffraction spectra for the holographic FZP were analyzed by angle-resolved measurements. The sample was mounted on a straight slot perpendicular to the light source in order to illuminate the sample normally. The framework for placing the sample and light source was supported on a 3D adjustable stage controlled by a stepper motor. The spectrometer was placed in alignment with the 3D stage, and it was able to rotate 360° with 1° increments. By rotating the 3D stage automatically, the intensity plot was recorded throughout the diffraction region (Figure 6a). The distance between the sample and spectrometer ranged from 8.7 to 21.8 cm in 2.5 cm intervals to detect the focal length in the visible light regime (blue to red).

Figure 6b illustrates the diffraction spectra at a distance of 6.2 cm as a function of rotational angle. The diffracted spectrum was between 400 and 800 nm with diffraction angles ranging from 34° to 68°. To obtain continuous diffraction spectra throughout the diffraction region, an interpolated curve was formed by connecting the peak intensity of each spectrum. The optical intensity of the green light region (492−577 nm) was the strongest among the diffraction pattern. The focal lengths for three wavelengths (455, 532, and 650 nm) were determined by measuring different diffracted intensities according to a series of

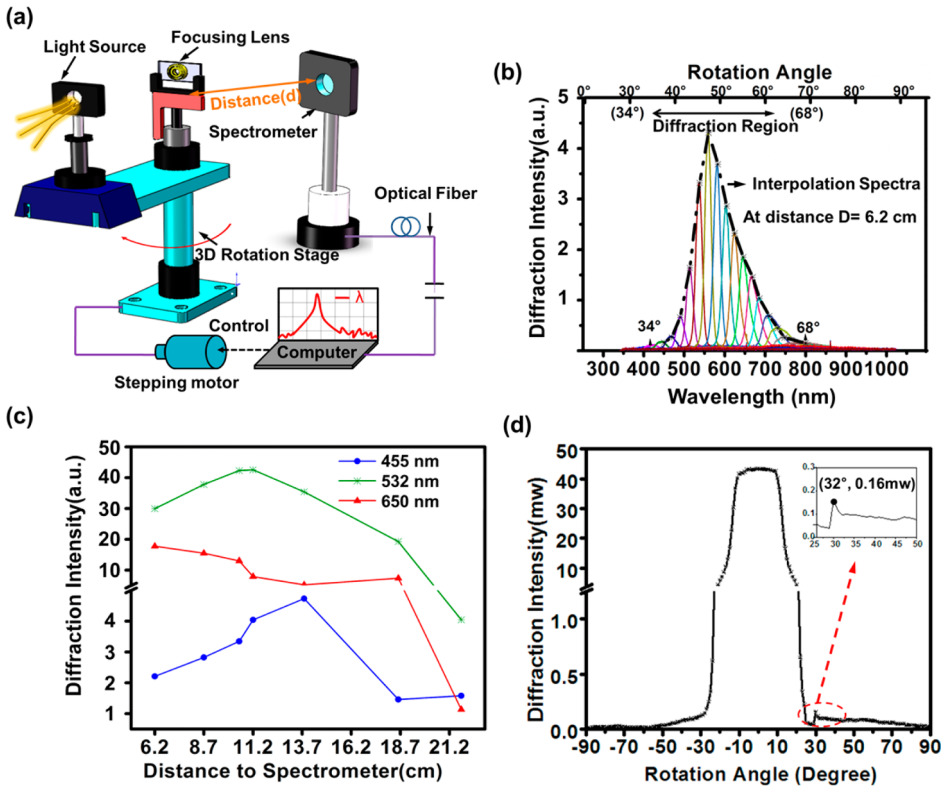

Figure 6. Angle-resolved measurements of the Fresnel zone plate. (a) Schematic setup for recording diffraction spectra. (b) Diffraction intensity under different wavelengths as a function of rotation angle at distance of 6.2 cm. (c) Diffraction intensity in response to 455, 532, and 650 nm light as the distance to the spectrometer was varied. (d) Diffracted intensity distribution as a function of 180° rotation corresponding to incident white light.

distances between the sample and spectrometer (Figure 6c). For 532 nm, the diffraction intensity was higher than that of 455 and 650 nm. The optical intensity was maximized when the distance was ~11.2 cm, which was the experimental focal length for the green ray. For 455 nm, the diffraction intensity increased up to the distance of ~13.8 cm and then decreased to a minimum at a distance of 21.8 cm; thus, the focal length for blue light was ~13.8 cm. The diffraction intensity for 650 nm decreased as distance was increased, showing a focal length of ~6.2 cm.

The diffraction efficiency was also measured by an optical power meter, which was placed at a distance of 18.3 cm from the holographic FZP. Figure 6d shows the intensity plot in response to rotation angle. The peak optical intensity was observed at 32° after the presence of the broadband light source, indicating a diffraction spot in transmission mode. This coincides with the diffraction angle measured in the spectroscopy experiment (Figure S3b). Additionally, there was a reflective spot in the reverse direction. The maximum diffraction efficiency for white light illumination was calculated to be 0.8% by adding two symmetric diffraction spots together (~0.4% for each spot).

DISCUSSION

We demonstrated a simple and rapid surface holographic patterning strategy to fabricate parallel surface gratings and FZPs consisting of a gold film (4.5 nm). In addition to the present work, recently several advances have been demonstrated in fabricating FZPs. FZPs can be created by forming voids or refractive index changes in bulk silica using femtosecond lasers.[22,23] However, this nonparallel laser patterning approach does not involve laser interference. Hence, it is slower and limited to micrometer scale resolutions. Recently, a FZP was fabricated *via* a focused Ga^+ ion beam.[24] While this approach enabled the fabrication of the FZP with a diffraction efficiency of ~9.7%, it required a high-cost setup and long fabrication times (>10 min) as compared to our strategy. Although accurate gratings can be fabrication *via* EBL and FIB approaches, they are time-consuming and costly and are not applicable to mass manufacturing. In the present work, Nd:YAG laser intensity was used to pattern gold in an area of 3 cm^2 within seconds, offering reduction both in cost and fabrication duration. While ~10 mJ energy is used to pattern gold, frequency doubling can achieve 350 mJ, which can be industrially scaled to ablate large areas. Hence, the present work demonstrates a practical and flexible approach for patterning parallel and radial gratings. The reproducibility of the grating periodicity is determined by the accuracy of controlling the tilt angle in the Denisyuk reflection setup, and the smallest resolution possible is around $\lambda/2$ (a few hundred nanometres) at tilt angles closer to 90°. A limitation

of the present work includes the requirement for transparent materials to pattern the grating because Denisyuk reflection mode requires the object beam to propagate through the substrate. This process also produces internal reflections from the gold−glass interface; however, the object beam is the main contributor to the grating formation as it passes the ablation threshold.[25] Another limiting factor for this approach could be the laser spot size uniformity. For larger patterned areas, multiple exposures can be adapted.

CONCLUSION

Our laser interference methodology has many attractive aspects due to its flexible and simple setup. While the present work employed gold as the recording medium, it does not have strong affinity to glass. This can be improved by functionalizing the surface with silane chemistry or coating the patterned surface with hydrophobic polymers. A diversity of well-ordered surface holograms may be produced by laser interference ablation on a variety of materials, such as inks, dyes, nanoparticles, and metallic coatings. Furthermore, our technique is applicable to different substrate materials, including transparent or opaque polymers or quartz, in flat, curved or arbitrary geometries. As shown by the experimental results, we can rapidly achieve mass production within a few minutes. Additionally, the diffraction angle displayed by asymmetric FZPs showed higher contrast as compared to conventional ones. The diffraction efficiency can be further enhanced by increasing the thickness of the deposited layer and using materials with a high refractive index. We anticipate that our strategy to fabricate surface holograms will have numerous applications in optical elements, security, data storage, and biosensors.

METHODS

Fabrication of the Gratings. Gold was evaporated over a microscope glass to obtain a ∼4.5 nm film with a transparency of ∼50%, and its absorption peak overlapped with the laser light used to produce the grating. Nd−Yttrium−Aluminum−Garnet pulsed laser (high-power compact Q-switched Nd:YAG oscillator with super Gaussian resonator, 700 mJ @ 1064 nm, 10 Hz) with a second harmonic generator, 350 mJ @ 532 nm 10 Hz, thermally stabilized with wavelength separation) was used to pattern gold. The parallel and radial surface gratings were patterned in in-line Denisyuk reflection mode. A plane dielectric mirror was placed on a leveled surface, and an incident beam was aligned to be normal to the surface plane. The gold-coated substrate was placed over the mirror with a tilt angle of 5° from the surface plane. The gold was patterned using 5 ns pulses (350 mJ, 532 nm, 10 Hz, a spot size of ∼1 cm in diameter) of the Nd:YAG laser beam. The laser energy patterning the gold film was measured as ∼10 mJ using a power meter. The radial gratings were created by replacing the plane mirror with a concave mirror, which had a diameter and radius of 2.5 and 6.2 cm, respectively.

Optical Characterization. The spectrometer (Ocean Optics) with an optical resolution of ∼0.1−100 nm full width at half-maximum was used to measure optical intensity with an integration time of 1 s to obtain the maximum peak intensity. COMSOL Multiphysics (v5.1) and MATLAB (MathWorks, v8.1) were used for data processing and finite element simulations.

Conflict of Interest: The authors declare no competing financial interest.

Acknowledgment. We thank Piran R. Kidambi for substrates. A.K.Y. and H.B. conceived the idea. A.K.Y. fabricated the gratings. H.B. and A.S. developed all the optical experimental setups, and Q.Z. and A.S. performed optical experiments. A.S. carried out the spectroscopy measurements and optical microscopy. A.K.Y. and Q.Z. analyzed data and wrote the manuscript. S.H.Y. and H.B. made intellectual contributions and edited the article. H.B. thanks the Leverhulme Trust for research funding.

Supporting Information Available: The Supporting Information is available free of charge on the ACS Publications website at DOI: 10.1021/acsnano.5b03165.

Optical measurement setups and optical microscopy images of the samples (PDF)

REFERENCES AND NOTES

1. Tay, S.; Blanche, P.-A.; Voorakaranam, R.; Tunc, A.; Lin, W.; Rokutanda, S.; Gu, T.; Flores, D.; Wang, P.; Li, G.; et al. An Updatable Holographic Three-Dimensional Display. *Nature* **2008**, *451*, 694–698.
2. Blanche, P.-A.; Bablumian, A.; Voorakaranam, R.; Christenson, C.; Lin, W.; Gu, T.; Flores, D.; Wang, P.; Hsieh, W.-Y.; Kathaperumal, M.; et al. Holographic Three-Dimensional Telepresence Using Large-Area Photorefractive Polymer. *Nature* **2010**, *468*, 80–83.
3. Yetisen, A. K.; Montelongo, Y.; da Cruz Vasconcellos, F.; Martinez-Hurtado, J. L.; Neupane, S.; Butt, H.; Qasim, M. M.; Blyth, J.; Burling, K.; Carmody, J. B.; et al. Reusable, Robust, and Accurate Laser-Generated Photonic Nanosensor. *Nano Lett.* **2014**, *14*, 3587–93.
4. Smalley, D.; Smithwick, Q.; Bove, V.; Barabas, J.; Jolly, S. Anisotropic Leaky-Mode Modulator for Holographic Video Displays. *Nature* **2013**, *498*, 313–317.
5. Yetisen, A. K.; Qasim, M. M.; Nosheen, S.; Wilkinson, T. D.; Lowe, C. R. Pulsed Laser Writing of Holographic Nanosensors. *J. Mater. Chem. C* **2014**, *2*, 3569–3576.
6. Farandos, N. M.; Yetisen, A. K.; Monteiro, M. J.; Lowe, C. R.; Yun, S. H. Contact Lens Sensors in Ocular Diagnostics. *Adv. Healthcare Mater.* **2015**, *4*, 792–810.
7. Yetisen, A. K.; Montelongo, Y.; Qasim, M. M.; Butt, H.; Wilkinson, T. D.; Monteiro, M. J.; Yun, S. H. Photonic Nanosensor for Colorimetric Detection of Metal Ions. *Anal. Chem.* **2015**, *87*, 5101–8.
8. Tsangarides, C. P.; Yetisen, A. K.; da Cruz Vasconcellos, F.; Montelongo, Y.; Qasim, M. M.; Wilkinson, T. D.; Lowe, C. R.; Butt, H. Computational Modelling and Characterisation of Nanoparticle-based Tuneable Photonic Crystal Sensors. *RSC Adv.* **2014**, *4*, 10454–10461.
9. Yetisen, A. K.; Butt, H.; da Cruz Vasconcellos, F.; Montelongo, Y.; Davidson, C. A.; Blyth, J.; Chan, L.; Carmody, J. B.; Vignolini, S.; Steiner, U.; et al. Light-Directed Writing of Chemically Tunable Narrow-Band Holographic Sensors. *Adv. Opt. Mater.* **2014**, *2*, 250–254.
10. Vasconcellos, F. d. C.; Yetisen, A. K.; Montelongo, Y.; Butt, H.; Grigore, A.; Davidson, C. A.; Blyth, J.; Monteiro, M. J.; Wilkinson, T. D.; Lowe, C. R. Printable Surface Holograms *via* Laser Ablation. *ACS Photonics* **2014**, *1*, 489–495.
11. Yetisen, A. K.; Naydenova, I.; da Cruz Vasconcellos, F.; Blyth, J.; Lowe, C. R. Holographic Sensors: Three-Dimensional Analyte-Sensitive Nanostructures and Their Applications. *Chem. Rev.* **2014**, *114*, 10654–96.
12. Naydenova, I.; Jallapuram, R.; Toal, V.; Martin, S. A Visual Indication of Environmental Humidity Using a Color Changing Hologram Recorded in a Self-Developing Photopolymer. *Appl. Phys. Lett.* **2008**, *92*, 031109.

13. Zacharovas, S. J.; Bakanas, R.; Adlienė, D.; Šeperys, R.; Narmontas, P.; Jankauskaitė, V. Holograms Recording with Pulsed Laser on Diazonaphthoquinone-Novolac-based Photoresists and Their Nanocomposites. *Opt. Eng.* **2014**, *53*, 097101–097101.
14. Butt, H.; Montelongo, Y.; Butler, T.; Rajesekharan, R.; Dai, Q.; Shiva-Reddy, S. G.; Wilkinson, T. D.; Amaratunga, G. A. Carbon Nanotube based High Resolution Holograms. *Adv. Mater.* **2012**, *24*, OP331–OP336.
15. Montelongo, Y.; Tenorio-Pearl, J. O.; Milne, W. I.; Wilkinson, T. D. Polarization Switchable Diffraction based on Subwavelength Plasmonic Nanoantennas. *Nano Lett.* **2014**, *14*, 294–298.
16. Marshall, O. P.; Chakraborty, S.; Khairuzzaman, M.; Beere, H. E.; Ritchie, D. A. Reversible Mode Switching in Y-coupled Terahertz Lasers. *Appl. Phys. Lett.* **2013**, *102*, 111105.
17. Zhao, Q.; Yetisen, A. K.; Anthony, C.; Fowler, W. R.; Yun, S. H.; Butt, H. Printable Ink Holograms. *Appl. Phys. Lett.* **2015**, *107*, 041115.
18. Guo, Z.; Ran, L.; Qu, S.; Liu, S.; Han, Y. Holographic Fabrication of Periodic Microstructures by Interfered Femtosecond Laser Pulses. In *Laser Pulses - Theory, Technology, and Applications*; Peshko, I., Ed.; INTECH: Rijeka, Croatia, 2012; pp 295−316.
19. Lasagni, A. F.; Acevedo, D. F.; Barbero, C. A.; Mücklich, F. One-Step Production of Organized Surface Architectures on Polymeric Materials by Direct Laser Interference Patterning. *Adv. Eng. Mater.* **2007**, *9*, 99–103.
20. Müller-Meskamp, L.; Kim, Y. H.; Roch, T.; Hofmann, S.; Scholz, R.; Eckardt, S.; Leo, K.; Lasagni, A. F. Efficiency Enhancement of Organic Solar Cells by Fabricating Periodic Surface Textures using Direct Laser Interference Patterning. *Adv. Mater.* **2012**, *24*, 906–910.
21. Zhai, T.; Zhang, X.; Pang, Z.; Dou, F. Direct Writing of Polymer Lasers using Interference Ablation. *Adv. Mater.* **2011**, *23*, 1860–1864.
22. Srisungsitthisunti, P.; Ersoy, O. K.; Xu, X. Laser Direct Writing of Volume Modified Fresnel zone plates. *J. Opt. Soc. Am. B* **2007**, *24*, 2090–2096.
23. Watanabe, W.; Kuroda, D.; Itoh, K.; Nishii, J. Fabrication of Fresnel zone plate Embedded in Silica Glass by Femtosecond Laser Pulses. *Opt. Express* **2002**, *10*, 978–983.
24. Keskinbora, K.; Grévent, C.; Eigenthaler, U.; Weigand, M.; Schütz, G. Rapid Prototyping of Fresnel Zone Plates *via* Direct Ga+ ion Beam Lithography for High-Resolution X-ray Imaging. *ACS Nano* **2013**, *7*, 9788–9797.
25. Yetisen, A. K.; Montelongo, Y.; Farandos, N. M.; Naydenova, I.; Lowe, C. R.; Yun, S. H. Mechanism of Multiple Grating formation in High-Energy Recording of Holographic Sensors. *Appl. Phys. Lett.* **2014**, *105*, 261106.